Enhancing Indoor-to-Outdoor mmWave Communication with Transparent Amplifying Intelligent Surface

Liu, Bin ; Wang, Qing; Pollin, Sofie

DOI
10.1109/ICC45041.2023.10279668

Publication date
2023

Document Version
Final published version

Published in
Proceedings of the ICC 2023 - IEEE International Conference on Communications

Enhancing Indoor-to-Outdoor mmWave Communication with Transparent Amplifying Intelligent Surface

Bin Liu*, Qing Wang†, and Sofie Pollin*
*Department of Electrical Engineering, KU Leuven, Belgium.
†Computer Science Department, Delft University of Technology, The Netherlands.
Email: bin.liu2@kuleuven.be, qing.wang@tudelft.nl, sofie.pollin@kuleuven.be

***Abstract*—This paper presents a novel transparent amplifying intelligent surface (TAIS) architecture for uplink enhancement in indoor-to-outdoor mmWave communications. The TAIS is an amplifier-based transmissive intelligent surface that can refract and amplify the incident signal, instead of only refracting it with adjustable phase shift by most passive reconfigurable intelligent surfaces (RIS). With advanced indium tin oxide film and printing technology, TAIS can be fabricated on the windows without any visual effects. This paper primarily focuses on exploiting the TAIS-based architecture to boost the uplink spectral efficiency (SE) in indoor-to-outdoor mmWave communications. By jointly optimizing the TAIS's phase shift matrix and transmit power of the user equipment, the uplink SE can be maximized by exploiting the nonlinearity in the TAIS's amplification process. The key point is that we drive the optimal phase shift matrix that maximizes the SE and deduces its closed-form representation. The SE maximization is then proved to be transferred to the transmit power optimization problem. Another important aspect is that we design a low-complexity algorithm to solve the problem using the difference of convex programming. Simulations show that our proposed TAIS can increase the SE by up to 32.6% as compared to its alternative methods.**

***Index Terms*—Reconfigurable intelligent surface, transparent amplifying intelligent surface (TAIS), spectral efficiency, indoor-to-outdoor communication, nonlinear amplification.**

I. Introduction

Various applications and vertical domain expansion emerging from the evolution of mobile broadband, e.g., virtual reality and augmented reality, require beyond-5G networks to provide better uplink qualities. In particular, over 80% of mobile uses rely on the indoor-to-outdoor communication [1]. With the standardization efforts in the 3GPP Rel-16 and Rel-17, the millimeter wave (mmWave) frequency band is introduced as the 5G new radio (NR) to accommodate the increasing spectrum and transmission demands [2]. Enhancing the uplink capability of indoor-to-outdoor mmWave communication is important for future wireless networks.

Enhancing the uplink capability in indoor-to-outdoor communication is challenging. One reason is that the radio waves from indoors to outdoors suffer from penetration losses greatly, in the order of 15 to 26 dB in sub-6 GHz and 35 to 53 dB for mmWave band [3]. Another reason is that UEs are powered by battery, and the additional penetration loss challenges the link budget of indoor UEs. Emerging applications such as extended reality (XR) have the requirements in both capacity and power saving as having been specified in 3GPP Rel-17. It is critical to boost the uplink capacity with efficient power saving of UEs for indoor-to-outdoor mmWave communication.

Relay or repeater, a node deployed between the base station (BS) and UEs, can improve the network capacity in buildings. 3GPP standardizes relays for different 5G use case scenarios, such as integrated access and backhaul in Rel-16 and Rel-17. However, relaying has several drawbacks, such as signal processing complexity, noise enhancement, and self-interference at the relay nodes. Recently, reconfigurable intelligent surfaces (RISs) have been proposed to intelligently control the wireless channels [4]. Passive RIS elements are man-made electromagnetic sensors that are controlled by integrated circuits to effectively adapt the wavefront characteristics such as phase, frequency, and even polarization of impinging signals. Moreover, RISs are configured to operate as anomalous reflectors or refactors that are not subject to the half-duplex constraint and self-interference, which typically exist in the amplify-and-forward relays. RIS has been studied in [5] to enhance indoor-to-outdoor communication, where the RIS is composed of a large number of chipless RFID sensors and built inside the wall with two outdoor and indoor antennas on both sides.

However, RIS can introduce the *multiplicative fading* effect, because the equivalent path loss between the transmitter-RIS-receiver link is the product of the path losses of the transmitter-RIS and RIS-receiver links, which could be much larger than that of the direct link [6]. To overcome this issue, Long *et al.* in [7] used active RIS where each element is assisted by active loads that reflect and amplify the incident signal. In [8], reflection-type power amplifiers (PAs) was integrated into RIS to amplify the reflected signals. However, most of the current active RIS studies evaluate the performance under the linear amplification process assumption. In practice, the amplification of PA is always *nonlinear*. When working in a saturation regime, PAs generate distortion – which is relevant to the input signal – and degrades the system performance.

In this paper, for the first time, we propose a *transparent amplifying intelligent surface (TAIS)* architecture for the indoor-to-outdoor mmWave communications, as illustrated in Fig. 1. This amplifier-based transmissive metasurface can refract and amplify the incident signal instead of only refracting it with the adjustable phase shift. Benefiting from the advanced indium tin oxide (ITO) film and printing technologies, TAIS can be fabricated on an *optically-transparent* ITO glass or graphene materials [9], which can be integrated into the windows

ICC 2023 - IEEE International Conference on Communications | 978-1-5386-7462-8/23/$31.00 ©2023 IEEE | DOI: 10.1109/ICC45041.2023.10279668

without visual effects. TAIS could be easily installed in an environment-friendly way and can match the surroundings, rather than being embedded in concrete walls like some RISs [5]. To analyze the TAIS's performance, we select the metric *uplink spectral efficiency (SE)* with the practical consideration of nonlinear amplification. The SE maximization objective is formulated by jointly optimizing the phase shift matrix of the TAIS and the transmit power of the UE. Below, we summarize the main contributions of this paper.

- We propose a first-of-its-kind transparent amplifying intelligent surface (TAIS) architecture for uplink enhancement of the indoor-to-outdoor mmWave communications. As an optically-transparent refractor that can be deployed on windows, TAIS can adjust the phase shift of impinging signals, perform beamforming and amplify the signals. Thus, TAIS can save the link budget of indoor UEs.
- We drive the optimal phase shift matrix that maximizes the uplink spectral efficiency and deduces its closed-form representation, where the PAs' nonlinearity is considered in the amplification process of TAIS. The SE maximization is proved to be transferred to the optimal transmit power optimization problem.
- We further design a low-complexity algorithm to obtain the optimal transmit power based on the difference of convex (DC) programming. Various simulations demonstrate that our proposed TAIS-enhanced indoor-to-outdoor mmWave communication can enhance the uplink capacity without sacrificing the link budgets of UEs.

Notations: The following notations are used throughout this paper. $\mathbf{a}$ and $\mathbf{A}$ stand for a vector and a matrix, respectively; The conjugate, transpose, conjugate transpose, determinant, and trace of $\mathbf{A}$ are represented by $\mathbf{A}^*$, $\mathbf{A}^T$, $\mathbf{A}^H$, $\det(\cdot)$ and $tr(\cdot)$, respectively; $|\cdot|$ denote modulus operation; $\odot$ denotes the element-wise product operation of a matrix; $\mathbb{E}[\cdot]$ is the expectation of a complex variable; $\mathbb{C}$ and represent the complex number; $\mathcal{CN}(\mu, \mathbf{\Sigma})$ denotes the complex multivariate Gaussian distribution with mean μ and variance $\mathbf{\Sigma}$.

II. TAIS-enhanced Indoor-to-Outdoor mmWave Communication

A. System Model

We consider a TAIS-enhanced indoor-to-outdoor communication system as shown in Fig. 1. The optical-transparent TAIS is deployed on the window to enhance the performance of the uplink transmission from the indoor UE to the outdoor BS. Because the TAIS is transparent, it does not affect much the visual effect of the window. Assume the BS is equipped with N receiving antennas and the UE has a single antenna. There are M active transmissive elements (TE) on the TAIS, where each element can reconfigure the incident signal from the UE with the desired phase shift and amplify the signal. The signal amplification is realized by a parametric power amplifier [10]. Let the diagonal matrix $\mathbf{\Theta} = \text{diag}(e^{\jmath\vartheta_1}, \cdots, e^{\jmath\vartheta_M}) \in \mathbb{C}^{M\times M}$ denote the phase shift matrix of the TAIS, where $\vartheta_m \in [0, 2\pi)$ is the phase shift of the TAIS's m-th element. The baseband

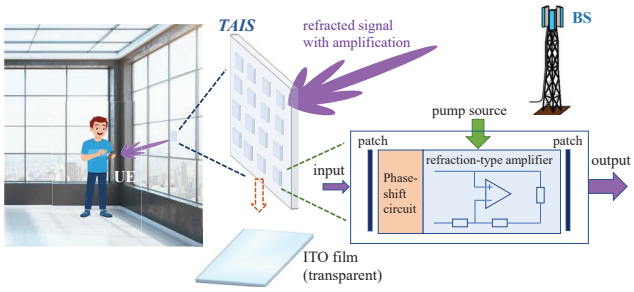

Fig. 1: Illustration of the proposed TAIS-enhanced indoor-to-outdoor mmWave communication scenario.

equivalent channels from the UE to the TAIS, and from the TAIS to the BS, are denoted by $\mathbf{h} \in \mathbb{C}^{M\times 1}$ and $\mathbf{F} \in \mathbb{C}^{N\times M}$, respectively. Following state-of-the-art studies [6]–[8], we assume the channel state information (CSI) of all the involved channels is known at the UE, BS, and TAIS. The received signal at the BS is given by

$$\mathbf{r} = \mathbf{F} f_A(\mathbf{\Theta}\mathbf{h}s) + \mathbf{n} = \mathbf{F} f_A(\mathbf{\Theta}\mathbf{x}) + \mathbf{n}, \tag{1}$$

where $\mathbf{x} = \mathbf{h}s = [x_1, \cdots, x_M]^{\mathrm{T}} \in \mathbb{C}^{M\times 1}$ denotes the incident signal at the TAIS; s is the transmitted signal by the UE with transmit power $\mathbb{E}[|s|^2] = P$; $f_A(\cdot) : \mathbb{C} \to \mathbb{C}$ is a function that describes the input and the output relationship of the signal amplification process at the TAIS; $\mathbf{n} \sim \mathcal{CN}(0, N_0\mathbf{I}_N)$ models the additive circularly symmetric complex Gaussian noise.

Remark. Note that our proposed TAIS is fundamentally different from the active relay-reflecting RIS described in [11]. Specifically, each element in the hybrid relay-reflecting RIS connects to a complete RF component, including the power amplifier and RF chain, enabling is signal processing capacity for the digital modulation of the signal in both amplitude and phase. Such active elements of a relay-reflecting RIS are used for sending pilot signals and estimating the channel state information [11] In contrast, our proposed TAIS is simpler, which does not perform fully digital modulation but only refracts and amplifies the incident signals. The signal amplification mechanism of TAIS is similar to the reflect-type amplifying surface [8], but TAIS is in a *refraction* manner.

B. Transmissive Amplifying Surface Model

Each element in the proposed TAIS can work as a refraction-type amplifier, which allows the refraction coefficient η greater than unity, i.e.,

$$|\eta|^2 = \frac{(R_L + R_A)^2 + (X_L + X_A)^2}{(R_L - R_A)^2 + (X_L + X_A)^2} > 1, \tag{2}$$

where R_L and R_A denote the resistance of the load and the antenna, respectively; X_L and X_A denote the reactance of the load and the antenna, respectively. It enables the elements to serve as a low-power refraction-type amplifier.

The low-power refraction amplifier, whose block diagram is illustrated in Fig. 2, can realize the power amplification with

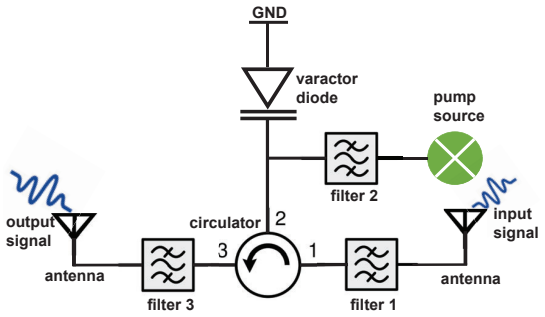

Fig. 2: Block diagram of a refraction-type amplifier.

a varactor diode circuit, three filters, and a pump source. An ideal impedance matching can be employed to realize such a single-port amplifier. The input signal power is amplified at the varactor diode, which can form a parametric amplifier based on the Manley–Rowe relations [12]. Filter 1 works for filtering out the undesired signal spectrum. Filter 2 works for the ideal operation of parametric amplification. In particular, it only allows the signal at the frequency of the pump source to pass through, which prevents mixing the input signal or the high-frequency component generated during the amplification process into the pump source. Filter 3 is used to filter out the undesired high-frequency component in the amplification, and only the amplified input signal at f_0 can pass through. The circulator can discriminate the input signal and the output signal during the amplification process. Due to the nonlinear property of the varactor diode, there exists a nonlinear operation region where the amplification gain is nonlinear while the phase is almost perfectly preserved [7].

C. Nonlinear Amplification Model

We adopt a memoryless polynomial model of $2K+1$ order to describe the non-linear behavior of PAs [13]. Denote by u_m the equivalent baseband output signal of the m-th PA that connects to the TE. Then, u_m is given by

$$u_m \triangleq \sum_{k=0}^{K} \beta_{2k+1} |v_m|^{2k} v_m, \tag{3}$$

where $v_m = [\mathbf{\Theta}]_{m,m} h_m s$ denotes the phase-modulated signal of the m-th TE. The β_{2k+1} is a model parameter that takes complex values in general. It can capture both amplitude-to-amplitude modulation (AM/AM) distortion and amplitude-to-phase modulation (AM/PM) distortion. The instantaneous amplitude gain of the PA is written as

$$g_m \triangleq \frac{u_m}{v_m} = \sum_{k=0}^{K} \beta_{2k+1} |v_m|^{2k}. \tag{4}$$

Let the diagonal matrix $\mathbf{G} = \mathrm{diag}(g_1, \cdots, g_M)$ be the instantaneous amplitude gain of each PA in (4), and $\mathbf{v} = \mathbf{\Theta} \mathbf{h} s$. Then, the amplified signal $\mathbf{u}$ can be represented as $\mathbf{u} = \mathbf{G}\mathbf{v}$.

D. Channel Model

1) Outdoor Channel Model: We consider a cluster channel model with L_2 paths in the outdoor scenario between the TAIS and the BS, and the channel matrix can be given by

$$\mathbf{F} = \sqrt{\frac{MN}{L_2}} \sum_{\ell=1}^{L_2} \alpha_\ell \mathbf{a}_r(\psi_\ell^B, \phi_\ell^B) \mathbf{a}_t^{\mathrm{H}}(\psi_\ell^{S_t}, \phi_\ell^{S_t}) \in \mathbb{C}^{N \times M}, \tag{5}$$

where α_ℓ is the complex gain of path ℓ between the TAIS and the BS, which includes both the path-loss and small-scale fading. In particular, for the given large-scale fading, $\{\alpha_\ell\}$ for all $\ell \in \{1, \cdots, L_2\}$ are i.i.d. random variables drawn from distribution $\mathcal{CN}(0, 10^{-0.1\mathrm{PL}_2})$, where PL_2 is the outdoor path-loss in dB. ψ_ℓ^B and ϕ_ℓ^B are the azimuth and elevation angles of arrival (AoA) of the BS; $\psi_\ell^{S_t}$ and $\phi_\ell^{S_t}$ are the azimuth and elevation angles of departure (AoD) of the TAIS, corresponding to path ℓ of the channel, respectively. $\mathbf{a}_t \in \mathbb{C}^{M \times 1}$ and $\mathbf{a}_r \in \mathbb{C}^{N \times 1}$ represent the unit-norm array response vectors of the BS and the TAIS arrays, respectively. We assume that both the BS and TAIS are equipped with uniform planar arrays (UPAs) with array responses as

$$\mathbf{a}_r(\psi, \phi) = \frac{1}{\sqrt{N_{az} N_{ev}}} \Big[1, \cdots, e^{-\jmath \frac{2\pi}{\lambda} \Delta_r (n_a \sin\psi \sin\phi + n_b \cos\phi)} \cdots, e^{-\jmath \frac{2\pi}{\lambda} \Delta_r ((N_{az}-1)\sin\psi \sin\phi + (N_{ev}-1)\cos\phi)}\Big]^T, \tag{6}$$

$$\mathbf{a}_t(\psi, \phi) = \frac{1}{\sqrt{M_{az} M_{ev}}} \Big[1, \cdots, e^{-\jmath \frac{2\pi}{\lambda} \Delta_t (m_a \sin\psi \sin\phi + m_b \cos\phi)} \cdots, e^{-\jmath \frac{2\pi}{\lambda} \Delta_t ((M_{az}-1)\sin\psi \sin\phi + (M_{ev}-1)\cos)}\Big]^T, \tag{7}$$

where $N = N_{az} N_{ev}$ and $M = M_{az} M_{ev}$. N_{az} and N_{ev} (M_{az}, M_{ev}) are the number of elements on each column and the row of the UPA at the BS (or TAIS), respectively. λ is the signal wavelength. Δ_t and Δ_r represent the antenna spacing of the arrays at the TAIS and the BS, respectively.

2) Indoor Channel Model: We consider a cluster channel model with L_1 paths between the TAIS and the UE in the indoor scenario. The channel matrix can be given by

$$\mathbf{h} = \sqrt{\frac{M}{L_1}} \sum_{\ell=1}^{L_1} \zeta_\ell \mathbf{a}_t(\psi_\ell^{S_r}, \phi_\ell^{S_r}) \in \mathbb{C}^{M \times 1}, \tag{8}$$

where ζ_ℓ is the complex gain of path ℓ between the TAIS and the UE, which includes both the path-loss and small-scale fading. In particular, for the given large-scale fading, $\{\zeta_\ell\}$ for all $\ell \in \{1, \cdots, L_1\}$ are i.i.d. random variables drawn from distribution $\mathcal{CN}(0, 10^{-0.1\mathrm{PL}_1})$, where PL_1 is the indoor path-loss in dB. $\psi_\ell^{S_r}$ and $\phi_\ell^{S_r}$ are the azimuth and elevation angles of arrival of the TAIS, corresponding to path ℓ of the channel, respectively.

III. Problem Formulation

In this section we analyze the uplink spectral efficiency (SE) of the proposed TAIS-enhanced indoor-to-outdoor mmWave links, where a realistic amplification process of TAIS is considered. Based on Bussgang's theorem, the amplified signal of TAIS can be represented as

$$\mathbf{u} = \overline{\mathbf{G}}\,\mathbf{v} + \mathbf{e} \in \mathbb{C}^M, \tag{9}$$

where $\mathbf{v}$ is the phase modulated signal at TAIS, and contaminated with the nonlinear distortion $\mathbf{e}$. $\overline{\mathbf{G}}$ denotes the average linear gain of the amplification. $\mathbf{e} = [e_1, \cdots, e_M]$ collects the nonlinear distortion over all the elements. According to the Bussgang's theorem, the distortion generated at the output of each PA is uncorrelated with the input signal to that PA, i.e., $\mathbb{E}\{v_m^* e_m\} = 0$. We assume that the element branches are isolated from each other. Hence, $\overline{\mathbf{G}}$ is assumed to be a diagonal matrix as

$$\overline{\mathbf{G}} = \mathrm{diag}\left(\overline{g}(P_1), \cdots, \overline{g}(P_M)\right), \tag{10}$$

where $P_m = |h_m e^{\jmath\vartheta_m}|^2 P$; $\overline{g}(P_m) = \sum_{k=0}^{K} \beta_{2k+1}(k+1)!|^{2k} P_m^k$ is the linear amplification gain. The details can be found in Appendix A. Then, by comparing with $\mathbf{u} = \mathbf{G}\mathbf{v}$ in (4), the nonlinear distortion can be expressed as $\mathbf{e} = \left(\mathbf{G} - \overline{\mathbf{G}}\right)\mathbf{v}$, where the nonlinear distortion vector $\mathbf{e}$ is a zero-mean complex random vector with covariance matrix

$$\mathbf{C_e} = \sum_{k=1}^{K} \mathbf{\Gamma}_k \mathbf{C_v} \odot |\mathbf{C_v}|^{2k} \mathbf{\Gamma}_k^H, \tag{11}$$

where $\mathbf{C_v} = \mathbb{E}\{\mathbf{v}\mathbf{v}^{\mathrm{H}}\} = P\mathbf{\Theta}\mathbf{h}\mathbf{h}^{\mathrm{H}}\mathbf{\Theta}^{\mathrm{H}}$ is the covariance matrix of signal vector $\mathbf{v}$. $\mathbf{\Gamma}_k = \mathrm{diag}\left(\gamma_k(P_1), \cdots, \gamma_k(P_M)\right)$, where

$$\gamma_k(P_m) = \sqrt{\frac{1}{k+1}} \sum_{q=k}^{K} \beta_{2k+1} \binom{q}{k} (q+1)! \left(|h_m e^{\jmath\vartheta_m}|^2 P\right)^{(q-k)}. \tag{12}$$

It can be obtained by the Isserlis' theorem [14].

Incorporating the impact of the PA's nonlinearity, the received signal at the BS in (1) can be updated as

$$\mathbf{r} = \mathbf{F}\overline{\mathbf{G}}\mathbf{v} + \mathbf{F}\mathbf{e} + \mathbf{n}. \tag{13}$$

When Gaussian symbols are transmitted from the UE to the BS, the SE of the uplink transmission is given by

$$SE = \log_2\left[\det\left(\mathbf{I}_N + \mathbf{R}_{\mathbf{n}}^{-1}\mathbf{F}\overline{\mathbf{G}}\mathbf{C_v}\overline{\mathbf{G}}^{\mathrm{H}}\mathbf{F}^{\mathrm{H}}\right)\right] \tag{14}$$

where $\mathbf{R_n} = \mathbf{F}\mathbf{C_e}\mathbf{F}^{\mathrm{H}} + N_0\mathbf{I}_N$.

As derived in (10) and (11), the linear amplification matrix $\overline{\mathbf{G}}$ and the covariance matrix of the distortion $\mathbf{C_e}$ depend on both the phase shift matrix $\mathbf{\Theta}$ of the TAIS and the transmit power P of the UE. Hence, the optimization problem is formulated as maximizing the SE by jointly optimizing the phase shift matrix of the TAIS and the transmit power of the UE, as follows:

$$\mathcal{P}_0: \max_{P,\mathbf{\Theta}} \quad SE(P, \mathbf{\Theta}) \tag{15a}$$

$$\text{s.t.} \quad 0 \le P \le P_{\max}, \tag{15b}$$

$$\mathbf{\Theta} = \mathrm{diag}\left(e^{\jmath\vartheta_1}, e^{\jmath\vartheta_2}, \cdots, e^{\jmath\vartheta_M}\right), \tag{15c}$$

where $P_{\max}$ is the maximum transmit power of the UE.

IV. Uplink SE Optimization

Problem $\mathcal{P}_0$ is challenging due to the nonconvexity of the objective function and the per-element unit modulus constraint placed on the phase shift matrix of the TAIS. In this section, we will derive the optimal phase shift matrix $\mathbf{\Theta}^*$ that maximizes SE under the considered indoor-to-outdoor scenario. Then, the SE maximization problem $\mathcal{P}_0$ is proved to be transferred to the optimal transmit power optimization problem. Finally, to further reduce the computational complexity, we design a low-complexity algorithm to obtain the solution using the difference of convex (DC) programming.

Considering in reality that the indoor distance d_1 is usually short, the maximum clearance of the first Fresnel zone can be written as [15]

$$d_F = \frac{1}{2}\sqrt{d_1\lambda}. \tag{16}$$

For example, at the typical mmWave frequency $f = 28$ GHz, the maximum clearance of the first Fresnel zone $d_F \approx 7.32$ mm for a typical indoor distance $d_1 = 2$ m. The surface with $M = 1000$ elements is about 8 mm in length, which means the power of the incidence signal on the surface is dominated by the strongest path of the indoor channel $\mathbf{h}$. Moreover, as indicated in the 3GPP clustered-delay-line (CDL) models [16], although multiple clusters may exist in the channel, the directed and narrow beam makes clusters in the other directions insignificant to the communication link. With these observations, the indoor channel characteristics can be approximately represented by its strongest path, as given by

$$\mathbf{h} \approx \sqrt{M}\zeta_{\max}\mathbf{a}_t(\overline{\psi}_{\max}^{S_r}, \overline{\phi}_{\max}^{S_r}) \triangleq \sigma_h\overline{\mathbf{h}} \in \mathbb{C}^{M\times 1}, \tag{17}$$

where $\psi_{\max}^{S_r}, \phi_{\max}^{S_r}$ are the azimuth and elevation angles of arrival at the TAIS that correspond to the strongest path with the largest channel gain $\zeta_{\max}$ in the indoor channel $\mathbf{h}$. For notation simplicity, let the complex channel gain $\sigma_h = \sqrt{M}\zeta_{\max}$, and $\overline{\mathbf{h}} = \mathbf{a}_t(\overline{\psi}_{\max}^{S_r}, \overline{\phi}_{\max}^{S_r})$. Then, the covariance matrix of the phase-modulated signal $\mathbf{v}$ can be rewritten as

$$\begin{aligned}\mathbf{C_v} &= \mathbb{E}\{\mathbf{v}\mathbf{v}^{\mathrm{H}}\} = P\sigma_h^2\mathbf{\Theta}\overline{\mathbf{h}}\overline{\mathbf{h}}^{\mathrm{H}}\mathbf{\Theta}^{\mathrm{H}} \in \mathbb{C}^{M\times M} \\ &\triangleq \rho\mathbf{\Theta}\overline{\mathbf{h}}\overline{\mathbf{h}}^{\mathrm{H}}\mathbf{\Theta}^{\mathrm{H}} \in \mathbb{C}^{M\times M},\end{aligned} \tag{18}$$

where $\rho = [\mathbf{C_v}]_{m,m} = \sigma_h^2 P$ is the average power of the phase-modulated signal feeding to the m-th PA.

In the following, we drive the optimal phase shift matrix $\mathbf{\Theta}^*$ that maximizes the SE, and deduce the closed-form maximum SE representation in Theorem 1.

Theorem 1. *The SE in* (14) *can be maximized if the optimal phase shift matrix of the TAIS* $\mathbf{\Theta}^*$ *satisfies*

$$\mathbf{\Theta}^*\overline{\mathbf{h}} = \sqrt{M}\mathbf{a}_t(\psi_{\max}^{S_t}, \phi_{\max}^{S_t}) \tag{19}$$

where $\psi_{\max}^{S_t}$*and* $\phi_{\max}^{S_t}$ *are the azimuth and elevation angles of departure of the TAIS corresponding to the path with the largest small-scale fading gain in the outdoor channel matrix* $\mathbf{F}$*. In other words, the optimal phase shift of the* m*-th element of the TAIS* ϑ_m^* *satisfies*

$$\vartheta_m^* = \angle\{\mathbf{a}_t(\psi_{\max}^{S_t}, \phi_{\max}^{S_t})\}_m - \angle\overline{h}_m, \tag{20}$$

where $\angle\{\mathbf{a}_t(\psi_{\max}^{S_t}, \phi_{\max}^{S_t})\}_m$ *and* $\angle\overline{h}_m$ *denote the angle of the* m*-th element of vector* $\mathbf{a}_t(\psi_{\max}^{S_t}, \phi_{\max}^{S_t})$ *and the channel* $\overline{\mathbf{h}}$ *in* (17)*, respectively. The maximum SE can be achieved as*

$$\overline{SE} = \left[\log_2\left|\mathbf{I}_N + \rho\overline{\gamma_s}(\rho)(N_0\mathbf{I}_N + \rho\overline{\gamma_e}(\rho)\overline{\mathbf{F}}\overline{\mathbf{F}}^{\mathrm{H}})^{-1}\overline{\mathbf{F}}\overline{\mathbf{F}}^{\mathrm{H}}\right|\right], \tag{21}$$

where $\overline{\mathbf{F}} = \sqrt{M}\mathbf{F}\mathbf{a}_t(\psi_{\max}^{S_t}, \phi_{\max}^{S_t})$*;* $\overline{\gamma}_s(\rho)$ *and* $\overline{\gamma}_e(\rho)$ *represent the linear and nonlinear power gains as*

$$\overline{\gamma}_s(\rho) \triangleq |\overline{g}(\rho)|^2 = \left|\sum_{k=0}^{K}\beta_{2k+1}(k+1)!\rho^k\right|^2, \tag{22}$$

$$\overline{\gamma}_e(\rho) \triangleq \sum_{k=1}^{K}|\gamma_k(\rho)|^2\rho^{2k}. \tag{23}$$

Proof. See Appendix B. □

As revealed in Theorem 1, $\overline{SE}$ only depends on the transmit power of the UE, if the optimal phase shift matrix $\mathbf{\Theta}^*$ is adopted at the TAIS. In this sense, the per-element unit modulus constraint can be removed. Hence, the maximum SE can be achieved by optimizing the transmit power of the UE in one-dimension. Problem $\mathcal{P}_0$ can be simplified as

$$\begin{aligned}\mathcal{P}_1: \max_{P} \quad & \overline{SE}(P) \\ \text{s.t.} \quad & 0 \le P \le P_{\max}.\end{aligned} \tag{24}$$

In this following, we propose a low-complexity DC-based method to obtain the solution of Problem $\mathcal{P}_1$. The key idea is to equivalently transform the optimization $\mathcal{P}_1$. The objective function after transformation is shown as the difference of the two convex functions. The new problem can be then iteratively solved by using DC programming [17].

First, $\mathcal{P}_1$ can be equivalently transformed to

$$\begin{aligned}\mathcal{P}_2: \max_{\rho} & \log_2\left(N_0 + \rho(\overline{\gamma_s}(\rho) + \overline{\gamma_e}(\rho))\overline{\mathbf{F}}^{\mathrm{H}}\overline{\mathbf{F}}\right) \\ & - \log_2\left(N_0 + \rho\overline{\gamma_e}(\rho)\overline{\mathbf{F}}^{\mathrm{H}}\overline{\mathbf{F}}\right) \\ \text{s.t.} \quad & 0 \le \rho \le \sigma_h^2 P_{\max},\end{aligned} \tag{25}$$

where the transformation of the objective function is achieved by using $\log_2\left|\mathbf{I}_N + \mathbf{A}\mathbf{B}^{-1}\right| = \log_2|\mathbf{A}+\mathbf{B}| - \log_2|\mathbf{B}|$ and the Weinstein–Aronszajn identity $|\mathbf{I}_N + \mathbf{A}\mathbf{B}| = |\mathbf{I}_M + \mathbf{B}\mathbf{A}|$.

Note that the objective function of Problem $\mathcal{P}_2$ can be viewed as a difference of two convex functions, denoted by $y_1(\rho) - y_2(\rho)$, and the feasible set of Problem $\mathcal{P}_2$ is convex. Now, we can solve Problem $\mathcal{P}_2$ by using DC programming. The main idea is to iteratively solve convex approximations of Problem $\mathcal{P}_2$ which is obtained by linearizing the function $y_2(\rho) = \log_2\left(N_0 + \rho\overline{\gamma_e}(\rho)\overline{\mathbf{F}}^{\mathrm{H}}\overline{\mathbf{F}}\right)$: Specifically, the convex approximation of Problem $\mathcal{P}_2$ at the i-th iteration is given by:

$$\begin{aligned}\mathcal{P}_3: \rho^{(i)} \triangleq \arg\max_{\rho} \; & y_1(\rho) - \hat{y_2}(\rho, \rho^{(i-1)}) \\ \text{s.t.} \quad & 0 \le \rho \le \sigma_h^2 P_{\max},\end{aligned} \tag{26}$$

where

$$\hat{y_2}(\rho, \rho^{(i-1)}) = y_2(\rho^{(i-1)}) + y_2'(\rho^{(i-1)})(\rho - \rho^{(i-1)}), \tag{27}$$

and $y_2'(\rho)$ is its derivative. Problem $\mathcal{P}_3$ is a convex optimization problem and can be solved using standard convex optimization techniques, e.g., the CVX tools.

V. Performance Evaluation

In this section, we evaluate the performance of the proposed TAIS-enhanced indoor-to-outdoor communication system in simulations. We simulate a system operating at $f_c = 28$ GHz. The number of antennas at the BS and the number of elements at TAIS are respectively configured as $N = 10$ and $M = 100$, unless specified otherwise. For the mmWave channels, we set the number of paths as $L_1 = L_2 = 10$; the azimuth and elevation angles of arrival and departure are randomly generated according to the Laplacian distribution with an angle spread of 10°; the complex gain follows the complex Gaussian distribution $\mathcal{CN}(0, 10^{-0.1PL_i(d)})$, $i \in \{1, 2\}$. The noise power is configured as $N_0 = -105$ dBm. Referring the path loss models for NLOS cases in the indoor (InH) environment, i.e., $PL_1(d_1)$, and outdoor (UMi) environment, i.e., $PL_2(d_2)$, are given as follows, respectively [3]:

$$PL_1(d_1)[\text{dB}] = 43.3\log_{10}(d_1) + 11.5 + 20\log_{10}(f_c), \tag{28}$$

$$PL_2(d_2)[\text{dB}] = 36.7\log_{10}(d_2) + 22.7 + 26\log_{10}(f_c), \tag{29}$$

where d_1 and d_2 are the distances between the TAIS and the UE and the BS, respectively. $\beta_1 = 2.96$, $\beta_3 = 448.41e^{-\jmath 2.816}$ and $\beta_5 = 3000e^{\jmath 0.39}$ [18].

We repeat the simulations $2,000$ times with independent channel realizations each time, and the simulation results are averaged. For comparison, we also evaluate the passive RIS with optimal phase shift matrix $\mathbf{\Theta}^*$ and passive RIS with random phase shift matrix $\mathbf{\Theta}$. For a fair comparison, for these two benchmarks with passive RIS, we assume that an extra amplification gain is added at the BS and is equal to 35 dB. We also evaluate the performance under an ideally linear power amplification assumption, which gives a high performance bound but is hard to achieve in reality.

Fig. 3 plots the spectral efficiency when the UE transmits with different power budget P. The distance from TAIS to UE and BS are $d_1 = 2.5$ m and $d_2 = 45$ m, respectively. We can observe the proposed TAIS outperforms the passive RIS system with the same transmit power of the UE, by optimal power and phase shifts optimization at TAIS. The passive RIS with optimal phase shift can achieve the maximum channel gain by beamforming, thus having a higher SE than

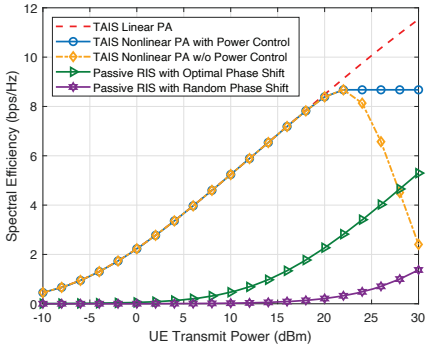

Fig. 3: Spectral efficiency under different UE transmit power P: $M = 100$, $d_1 = 2.5$ m, $d_2 = 45$ m.

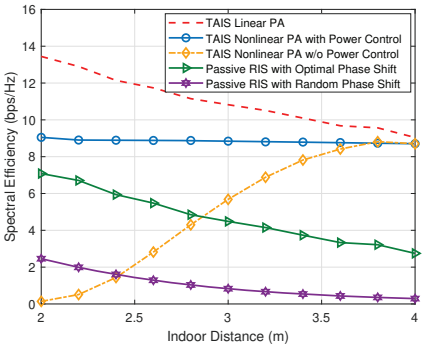

Fig. 4: Spectral efficiency under different distance between UE and TAIS d_1: $M = 100$, $d_2 = 45$ m, $P = 20$ dBm.

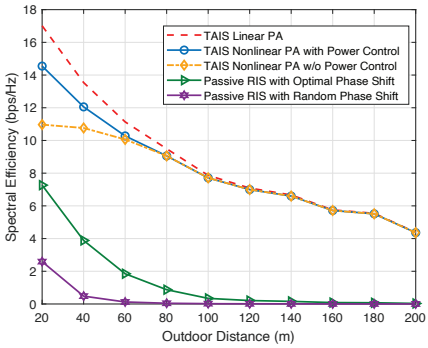

Fig. 5: Spectral efficiency under different distance between BS and TAIS d_2: $M = 10$, $d_1 = 2.5$ m, $P = 20$ dBm.

its counterpart with random phase shifts. The huge path loss causes the weak direct link from indoor to outdoor, resulting in a low uplink transmission SE for the case of passive RIS in indoor-to-outdoor communications.

Another observation from Fig. 3 is that the SE non-monotonically increases with the input power due to the presence of nonlinear distortion. The SE increases with the transmit power of the UE when $P < 20$ dBm, where the amplification is in the linear region. However, instead of having a linear increase with input power (red dash line in Fig. 3) as shown in [8], the SE degrades when $P > 20$ dBm. The reason is that the SE decreases with the increase of transmit power when the distortion dominates the SE performance. Therefore, the UE's transmit power needs to be meticulously optimized to avoid the distortion and maximize the SE.

We further evaluate the spectral efficiency when the UE is located at difference indoor distances (d_1) to the TAIS. The results are shown in Fig. 4. It is observed that SE decreases with d_1 due to path loss. In particular, the SE of TAIS is lower than the passive RIS when the UE's indoor distance is small. In this case, the power of the incidence signal on the TAIS is large and distorts the signal during the amplification process, even with optimal power control at the TAIS. Without power control at the TAIS, SE decreases rapidly since the distortion grows larger and degrades the performance when UE is closer to the TAIS. As observed, when the UE is far from the TAIS, the power level of the incidence signal is lower and PA works in approximately linear region, which exhibits a similar SE performance regardless of power control or the linear PA assumption.

Fig. 5 plots the spectral efficiency under different outdoor distance d_2 to the BS. It is observed that SE is low when the BS is far from the building (or TAIS) due to the huge path loss incurred when the mmWave signal propagates through the outdoor environment. It is also confirmed that the TAIS and the RIS should be deployed either close to UE or BS due to the product effect of the outdoor and indoor channels, as shown in [8]. The proposed TAIS can achieve higher SE by amplifying the signal with a larger beamforming gain. In particular, by jointly optimizing the input power and phase shift at TAIS, 32.6% and 200% SE improvement can be achieved when $d_2 = 20$ m, compared with other two benchmarks.

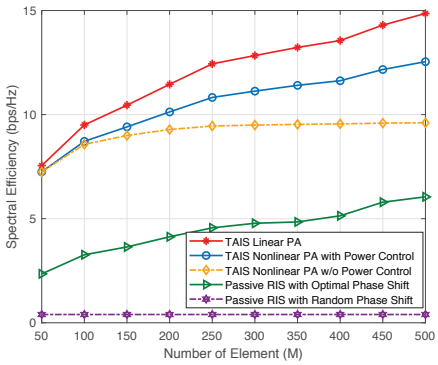

Fig. 6: Spectral efficiency versus different number of elements on TAIS M: $P = 22$ dBm, $d_1 = 2.5$ m, $d_2 = 45$ m.

Fig. 6 plots the spectral efficiency versus the number of elements M on the TAIS (or RIS for the two benchmarks). The SE of both TAIS and RIS improves as the number of elements M increases. It is because a larger channel gain can be achieved with an optimal phase shift matrix applied at either TAIS or passive RIS, which is proportional to the number of elements M. By contrast, the passive RIS with random phase shift cannot benefit from the increased elements M. In addition to larger channel gain, the TAIS achieves higher SE due to the signal amplification. We also observe that the SE of the TAIS degrades when power control at UE is not adopted, where the distortion increases and degrades SE performance.

VI. Conclusion

In this paper, we proposed a novel transparent amplifying intelligent surface (TAIS) architecture for uplink enhancement in indoor-to-outdoor mmWave communication. TAIS is an optically-transparent refractor integrated with the window, and can adjust the phase shift of an impinging signal, perform beamforming and amplify the signal, thus enhancing the

network service for indoor UEs. A SE maximization problem was structured by jointly optimizing the phase shift matrix of the TAIS and the transmit power of the UE. Considering PAs' nonlinearity in TAIS, we proved the optimal phase shift matrix that maximizes the spectral efficiency, deduces its closed-form representation, and thus transfer SE maximization to transmit power optimization problem. Moreover, a power optimization algorithm was established based on the DC programming, with significantly low complexity. Extensive simulations demonstrated that our approach can boost the uplink capacity with efficient energy saving of indoor UEs.

APPENDIX A
DERIVATION OF LINEAR POWER GAIN

From (9), the amplified signal at the m-th element of TAIS is given as $u_m = \bar{g}_m\, v_m + e_m$. By using the Bussgang theorem, the average linear amplification gain can be written as

$$\begin{aligned}\bar{g}_m =& \frac{\mathbb{E}\{u_m v_m^*\}}{\mathbb{E}\{|v_m|^2\}} \overset{(a)}{=} \frac{1}{P_m}\mathbb{E}\left\{\sum_{k=0}^{K}\beta_{2k+1}\left|v_m\right|^{2k+2}\right\} \\ =& \sum_{k=0}^{K}\beta_{2k+1}(k+1)!P_m^k. \end{aligned} \tag{30}$$

where the equation (a) is by the fact that the distortion is uncorrelated with the linear signal, i.e., $\mathbb{E}\{v_m e_m^*\} = 0$.

APPENDIX B
PROOF OF THEOREM 1

We prove Theorem 1 by leveraging Lemma 1. Define $\mathbf{X}$ and $\mathbf{X}'$ as two positive semi-definite (PSD) matrices with dimension of R, Denote $\mathbf{X}' \succeq \mathbf{X}$, if $\mathbf{X}' - \mathbf{X}$ is a PSD matrix.

Lemma 1. *For the following function*

$$y(\mathbf{X}) = \log_2 \det\left(\mathbf{I} + \left(\omega_2\mathbf{X} + \mathbf{I}\right)^{-1}\omega_1\mathbf{X}\right), \tag{31}$$

if $\mathbf{X}' \succeq \mathbf{X}$*, we have* $y(\mathbf{X}') \geq y(\mathbf{X})$.

Proof. Rearrange the eigenvalues of $\mathbf{X}$ and $\mathbf{X}'$ in descending order, $\lambda_1 \geq \cdots \geq \lambda_r$ and $\lambda_1' \geq \cdots \geq \lambda_r'$, respectively. Since that $\mathbf{X}' \succ \mathbf{X}$, we have each eigenvalue $\lambda_r \geq \lambda_r'$ for $r = 1, \cdots, R$. $y(\mathbf{X})$ can be equivalently expressed as the function of the eigenvalues of the matrix $\mathbf{X}$, as follows

$$y(\mathbf{X}) = \sum_{r=1}^{R}\log_2\left(1 + \frac{\omega_1\lambda_r}{\omega_2\lambda_r + 1}\right), \tag{32}$$

which is a non-decreasing function of λ_r. Therefore, we have $y(\mathbf{X}') \geq y(\mathbf{X})$, since $\lambda_r \geq \lambda_r'$, $\forall r = \{1, \cdots, R\}$. □

Since the input power of each PA is equal to ρ, we have the matrix of the average linear gain as $\overline{\mathbf{G}} = \overline{g}\left(\rho\right)\mathbf{I}_M$, and the numerator in the SE expression (14) is given by

$$\overline{\mathbf{G}}\mathbf{C}_{\mathbf{v}}\overline{\mathbf{G}}^{\mathrm{H}} = \overline{\gamma}_s(\rho)\rho\ \boldsymbol{\Theta}\mathbf{h}\mathbf{h}^{\mathrm{H}}\boldsymbol{\Theta}^{\mathrm{H}}. \tag{33}$$

The covariance matrix of the distortion in (11) is updated as

$$\mathbf{C}_{\mathbf{e}} = \sum_{k=1}^{K}|\gamma_k(\rho)|^2\rho^{2k}\mathbf{C}_{\mathbf{v}} = \overline{\gamma}_e\left(\rho\right)\rho\ \boldsymbol{\Theta}\mathbf{h}\mathbf{h}^{\mathrm{H}}\boldsymbol{\Theta}^{\mathrm{H}}. \tag{34}$$

It is observed that the desired signal and distortion have the same spatial directivity. By substituting the ω_1 and ω_2 in (31) with $\overline{\gamma}_s\left(\rho\right)\rho/N_0$ and $\overline{\gamma}_e\left(\rho\right)\rho/N_0$, respectively, the SE in (14) can be written as $SE = y(\mathbf{F}\mathbf{C}_{\mathbf{v}}\mathbf{F}^{\mathrm{H}})$. $\rho\overline{\mathbf{F}}\overline{\mathbf{F}}^{\mathrm{H}} \succeq \mathbf{F}\mathbf{C}_{\mathbf{v}}\mathbf{F}^{\mathrm{H}}$ holds for any $\mathbf{C}_{\mathbf{v}} = \rho\boldsymbol{\Theta}\mathbf{h}\mathbf{h}^{\mathrm{H}}\boldsymbol{\Theta}^{\mathrm{H}}$, when the power constraint $tr(\mathbf{C}_{\mathbf{v}}) \leq \rho$ is met. Based on Lemma 1, we have $y(\rho\overline{\mathbf{F}}\overline{\mathbf{F}}^{\mathrm{H}}) \geq y(\mathbf{F}\mathbf{C}_{\mathbf{v}}\mathbf{F}^{\mathrm{H}})$, where the equality is achieved on the condition that $\boldsymbol{\Theta}\overline{\mathbf{h}} = \sqrt{M}\mathbf{a}_t(\psi_{\max}^{S_t}, \phi_{\max}^{S_t})$.

REFERENCES

[1] A. Schumacher, R. Merz, and A. Burg, "Adding indoor capacity without fiber backhaul: An mmWave bridge prototype," *IEEE Commun. Mag.*, vol. 59, no. 4, pp. 110–115, 2021.

[2] M. Giordani, M. Polese, A. Roy, D. Castor, and M. Zorzi, "Standalone and non-standalone beam management for 3GPP NR at mmWaves," *IEEE Commun. Mag.*, vol. 57, no. 4, pp. 123–129, 2019.

[3] 3GPP, "Study on channel model for frequencies from 0.5 to 100 GHz," Technical Report 38.901, January 2020.

[4] M. Di Renzo *et al.*, "Smart radio environments empowered by reconfigurable intelligent surfaces: How it works, state of research, road ahead," *IEEE J. Sel. Areas Commun.*, vol. 38, no. 11, pp. 2450–2525, 2020.

[5] M. Nemati, B. Maham, S. R. Pokhrel, and J. Choi, "Modeling RIS empowered outdoor-to-indoor communication in mmWave cellular networks," *IEEE Trans. Commun.*, vol. 69, no. 11, pp. 7837–7850, 2021.

[6] Q. Wu and R. Zhang, "Intelligent reflecting surface enhanced wireless network via joint active and passive beamforming," *IEEE Trans. Wireless Commun.*, vol. 18, no. 11, pp. 5394–5409, 2019.

[7] R. Long, Y.-C. Liang, Y. Pei, and E. G. Larsson, "Active reconfigurable intelligent surface-aided wireless communications," *IEEE Trans. Wireless Commun.*, vol. 20, no. 8, pp. 4962–4975, 2021.

[8] Z. Zhang *et al.*, "Active RIS vs. passive RIS: Which will prevail in 6G?" *arXiv preprint arXiv:2103.15154*, 2021.

[9] D. Kitayama *et al.*, "Transparent dynamic metasurface for a visually unaffected reconfigurable intelligent surface: controlling transmission/reflection and making a window into an RF lens," *Optics Express*, vol. 29, no. 18, pp. 29 292–29 307, 2021.

[10] J. Aumentado, "Superconducting parametric amplifiers: The state of art in Josephson parametric amplifiers," *IEEE Microw. Mag.*, vol. 21, no. 8, pp. 45–59, 2020.

[11] R. Schroeder, J. He, G. Brante, and M. Juntti, "Two-stage channel estimation for hybrid RIS assisted MIMO systems," *IEEE Trans. Commun.*, vol. 70, no. 7, pp. 4793–4806, 2022.

[12] A. Popov and V. M. Shalaev, "Negative-index metamaterials: second-harmonic generation, manley–rowe relations and parametric amplification," *Applied Physics B*, vol. 84, no. 1, pp. 131–137, 2006.

[13] N. Moghadam *et al.*, "On the energy efficiency of MIMO hybrid beamforming for millimeter-wave systems with nonlinear power amplifiers," *IEEE Trans. Wireless Commun.*, vol. 17, no. 11, pp. 7208–7221, 2018.

[14] L. Isserlis, "On a formula for the product-moment coefficient of any order of a normal frequency distribution in any number of variables," *Biometrika*, vol. 12, no. 2, pp. 134–139, 1918.

[15] Y. Hmamouche, M. Benjillali, and S. Saoudi, "Fresnel line-of-sight probability with applications in airborne platform-assisted communications," *IEEE Trans. Veh. Technol.*, vol. 71, no. 5, pp. 5060–5072, 2022.

[16] 3GPP, "Study on channel model for frequencies from 0.5 to 100 GHz," 3rd Generation Partnership Project (3GPP), Technical Report (TR), 2017. [Online]. Available: https://www.3gpp.org/DynaReport/38901.htm

[17] T. a. Lipp, "Variations and extension of the convex–concave procedure," *Optimization and Engineering*, vol. 17, no. 2, pp. 263–287, 2016.

[18] S. R. Aghdam *et al.*, "Distortion-aware linear precoding for millimeter-wave multiuser MISO downlink," in *Proc. IEEE Int. Conf. Commun. Workshops (ICC Workshops)*, 2019, pp. 1–6.